Article │ Received 13 December 2024; Accepted 13 March 2025; Published 7 April 2025
https://doi.org/10.55092/am20250007

Creating custom 3D printing material colors using optical modeling of waste plastic

Kimia Aghamohammadesmaeilketabforoosh[1], Joshua Givans[1], Morgan Woods[2] and Joshua M. Pearce[1,3,*]

[1] Department of Electrical & Computer Engineering, Western University, ON N6A 3K7 London, Canada
[2] Department of Mechanical and Materials Engineering, Spencer Engineering Building, Western University, ON N6A 5B9 London, Canada
[3] Ivey School of Business, Western University, ON N6A 3K7 London, Canada

* Correspondence author; E-mail: joshua.pearce@uwo.ca.

Highlights:

- Distributed recycling and additive manufacturing (DRAM) offers a path to a circular economy.
- Custom colors can increase value of DRAM polymers.
- Open-source software named SpecOptiBlend developed to target specific recycled plastic colors.
- Waste plastic spectral reflectance taken, Kubelka-Munk theory initial estimate for color mixing.
- Nelder-Mead method gave optimal balance between precision of color differences and RMS.

Abstract: Distributed recycling and additive manufacturing (DRAM) offer a unique promise for obtaining a circular economy. To maintain or even enhance the value of common 3D printing feedstocks like polylactic acid (PLA) waste an approach to further incentivize prosumers to use recycled feedstocks is to provide something the market currently does not—custom filament colors. To enable prosumers to create custom colors from their own recycled 3D printing waste this article presents a new open-source software named SpecOptiBlend. Specifically, this study introduces a novel method for customizing color filaments by recycling waste 3D printing samples, thereby enhancing the capabilities of color 3D printing. Traditional 3D printing is limited by a narrow range of filament colors, and even multi-color printing heads can utilize only a limited number of colored filaments among the available options. The new approach here repurposes discarded prototypes and unused samples back into the printing cycle with desired colors, allowing for a broader spectrum of colors and gradients. This enables engineers and designers to create more intricate and functionally graded materials. To do this, waste plastics are quantified after processing for spectral reflectance, then Kubelka-Munk theory provides the initial estimate for color mixing. Three discrete optimization techniques are applied: Nelder-Mead, Limited-memory BFGS with bounds, and Sequential Least

Squares Quadratic Programming. To determine the optimal method, assessment criteria include the application of root mean square (RMS) and the color difference (ΔE CIE-2000). Three case studies were conducted, and the Nelder-Mead method was found to provide an optimal balance between the precision of color differences and the RMS, essential for producing high-quality colors. This research has provided a free tool that will now enable prosumers to convert their plastic waste into specific custom colors to enable DRAM.

Keywords: waste plastic; opaque paints; color matching; spectroscopy; 3D printing

1. Introduction

Although materials extrusion 3D printing was historically used primarily for rapid prototyping, the creation of the open source self-replicating rapid (RepRap) [1–3] prototyper project reduced costs [4] to such a degree that true distributed manufacturing using commons-based peer production was possible [5]. In this model, prosumers (a portmanteau of producing consumers) [6,7] are able to select from millions of open source 3D printable designs and digitally replicate finished products for themselves using fused filament fabrication (FFF). As distributed production is so much more economically efficient, prosumers can easily justify the costs of desktop 3D printers by manufacturing only one product a week [8] for common household items over a year. In some cases the simple payback time is reduced to a weekend for specific products like scientific [9] or medical tool [10–12], a piece of an expensive hobby equipment like drones [13,14], or sporting goods [15]. Distributed 3D printing of high end tools and models is already supported by the NIH 3D Print Exchange [16,17] but also NASA 3D Resources and the Smithsonian X3D [18]. Prosumers are creating products for children from toys [19] and educational aids [20] to products for geriatrics like arthritic aids [21]. Based on downloaded substitution value and the number of downloads prosumers are already savings millions of dollars [22].

Unsurprisingly the global 3-D printing market is expanding rapidly and is expected to reach $7.7 billion by 2024 [23]. As the number of RepRap-class 3D printers and compatible designs has exploded there have become concerns about the increasingly significant amount of 3D printing plastic waste, particularly of the most popular 3D printing plastics like polylactic acid (PLA) and polyethylene terephthalate glycol (PETG) being landfilled [24]. One approach to moving 3D printing waste into a circular economy [25] is to use distributed recycling for additive manufacturing (DRAM) [26]. Unlike traditional recycling that fails to provide economic incentives for consumers to recycle plastic DRAM enables consumers to save money by offsetting additive manufacturing (AM) feedstock, which costs ~$20/kg with their own waste. DRAM generally uses a type of recyclebot (waste plastic extruder) [27] to manufacture filament for FFF. DRAM has been demonstrated successfully with PLA [27,28] and PETG [29] and can provide 98% savings when used for replacing purchased products [22]. An issue, however, is that with each DRAM cycle the mechanical properties of the PLA [30] and PETG [29] degrade making it a lower value feedstock. To maintain or even enhance the value of PLA or PETG waste an approach to further incentivizing prosumers to use recycled feedstocks is to provide something the market currently does not—custom filament colors. Although the market provides dozens of filament colors, prosumers are limited to these colors, or the generally aesthetically displeasing colors that are the result of mixing many wastes [31].

Color plays a pivotal role in both the aesthetic appeal and functional performance of 3D printed objects [32]. For example, matte black filaments are often used for optics components to reduce spectral errors from reflections. Traditional 3D printing methods often rely on a narrow palette of filament colors, which restricts the ability to replicate complex designs with accurate color fidelity. Moreover, discrepancies between intended and actual colors can affect not only the appearance, but also the functional properties of printed components, such as light absorption, thermal properties, and even mechanical strength in functionally graded materials [33].

Material extrusion in FFF involves the deposition of thermoplastic materials layer by layer to build objects. The molding principles of FFF are influenced by factors such as filament composition, extrusion temperature, nozzle diameter, and layer height, all of which can impact the final appearance and mechanical properties of the printed object. In terms of color reproduction, these factors play a critical role in how colors blend and how consistent the coloration is throughout the object. For instance, variations in extrusion temperature can cause color shifts due to thermal degradation of pigments or dyes within the filament [32]. In DRAM, the data flow characteristics involve the digital management of design files, material properties, and process parameters to ensure consistent production across decentralized locations [34]. Creation of specific colors based on the recycled plastics has never, however, been a target.

To enable the potential to create custom colors from their own recycled 3D printing waste this article presents a new open-source software named SpecOptiBlend [35]. In SpecOptiBlend approach, the objective is to create a specific color through the mixture of various waste plastic constituents. Initially, individual waste plastics undergo shredding, and compression molding for quantification of their spectral reflectance. Then Kubelka-Munk theory [36] provides the initial estimate for optimization procedures. Then, three discrete optimization techniques are applied to determine the most suitable proportions of each color within the composite. These optimization methods consist of one primary Python library [37]. The methods involve the utilization of the “minimize” function from the SciPy library [38], employing three minimization techniques, namely Nelder-Mead [39], Limited-memory BFGS with bounds [40], and Sequential Least Squares Quadratic Programming [41]. To determine the optimal method, assessment criteria include the application of root mean square (RMS) and the color difference (DELTAE). First, RMS assesses a model’s prediction accuracy by measuring the average difference between predicted and actual values [42]. Second, DELTA E CIE-2000 [43], which is a standard measurement by the CIE (Commission Internationale de l’Eclairage, International Commission on Illumination) [44], quantifies color differences. CIE2000 is derived from CIELAB and incorporates weighting functions for lightness, chroma, and hue. Additionally, it features an interaction term between chroma and hue differences to enhance accuracy for blue shades, and a scaling factor for the CIELAB a* scale to boost performance when dealing with gray shades [45]. The preferred optimization method is determined by selecting the one with the lowest values in both metrics when they are computed through various optimization approaches. In this study, reflectance data from recycled 3D printed waste was processed and subjected to optimizations using a Python library, SciPy, and the Kubelka-Munk theory was employed to assess the initial proportions for commencing the optimization process. To identify the optimal algorithm, three distinct colors were selected as case studies and replicated using the reflectance data of available waste plastic materials.

2. Background

Equation 1 illustrates the methodology for measuring DELTAE CIE2000. These metrics serve as reliable indicators of precision.

$$\Delta E_{2000} = \sqrt{\left(\frac{\Delta L^{'}}{K_L S_L}\right)^2 + \left(\frac{\Delta C^{'}}{K_c S_c}\right)^2 + \left(\frac{\Delta H^{'}}{K_H S_H}\right)^2 + R_T \left(\frac{\Delta C^{'}}{K_c S_c}\right)\left(\frac{\Delta H^{'}}{K_H S_H}\right)} \quad (1)$$

$\Delta L^{'}$, $\Delta C^{'}$, and $\Delta C^{'}$indicate the difference in lightness, chroma, and hue, respectively. $K_{L,}$ K_C, and K_H are weighting factors for the lightness, chroma, and hue differences, respectively. S_L, S_C, and S_H are scaling factors for the respective terms and are used to adjust the sensitivity of the formula to lightness, chroma, and hue variations. They are based on the average values of lightness, chroma, and hue for the two samples being compared. R_T is a rotation term that accounts for the interaction between chroma and hue differences in the blue regions of the color space.

To blend waste plastics to reproduce a specific color the principles of subtractive color mixing are used. Subtractive color mixing takes place when a light source interacts with tangible substances like dyes. During this process, specific portions of the light spectrum are absorbed, while the remaining portions are reflected for human visual perception. For instance, when we consider red pigment, it absorbs all segments of the visible spectrum except for the red portion, which results in the perception of the color red. Subtractive color mixing is a complex process involving colorants and concentrations to create specific colors, which presents a significant predictive challenge [46]. Berns introduced a two-step approach: a linear model for spectral data and colorant components, emphasizing scalability and additivity, and linking user controls to colorant quantity to improve color mixing comprehension [47]. Figure 1 shows subtractive mixing.

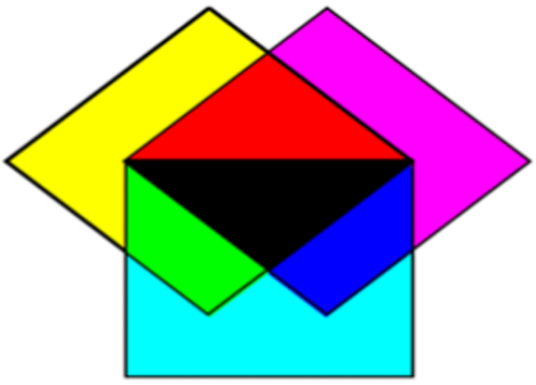

Figure 1. Subtractive mixing of colors.

Kubelka–Munk theory [48] has found application in modeling opaque paint mixtures, which is the closest analog for filament coloring. In this approach, the absorption and scattering characteristics of each colorant are employed to establish in a linear model. The equation for the two-constant Kubelka–Munk theory, featuring two independent scattering and absorption units for each color, is presented in equation 2:

$$\left(\frac{K}{S}\right)_{\lambda,\text{mixture}} = \frac{c_{e,1}k_{\lambda,1} + c_{e,2}k_{\lambda,2} + c_{e,3}k_{\lambda,3} + \cdots}{c_{e,1}s_{\lambda,1} + c_{e,2}s_{\lambda,2} + c_{e,3}s_{\lambda,3} + \cdots} \quad (2)$$

Here, k_λ and s_λ represent the absorption (dB) and scattering (m^2) characteristics of a colorant at a standardized quantity, while $c_{e,1}$ signifies the precise amount of each colorant. The choice of measurement units for these colorants may vary depending on the initial physical state of the samples. In this particular case, as the samples consist of ground plastics, the unit of measurement adopted is grams. Furthermore, the conversion from the reflectance factor to the $k/s_{\lambda,mixture}$ of each blend is depicted by:

$$\left(\frac{K}{S}\right)_{\lambda,mixture} = \frac{\left(1 - R_{\lambda,i}\right)^2}{2R_{\lambda,i}} \tag{3}$$

Through the process of combining precise quantities of individual colorants, measuring the resulting reflectance, and applying these mathematical formulations, a foundational framework will be established for initiating an optimization procedure aimed at determining the absorption and scattering coefficients of each colorant. Subsequently, this leads to the creation of a comprehensive tint ladder, encompassing various mixtures of individual colors and white colorants, each characterized by distinct concentration ratios [49].

To optimize this process, one effective approach involves employing the method of linear least squares [50]. This method entails generating various combinations of individual colorants and white substrate/colorant pairs, thereby establishing distinct linear equations for scattering and absorption properties of each mixture. Equations 4–6 illustrate an example of such a matrix equation. Through optimization, the values of K (absorption) and S (scattering) for each of the primary colorants can be derived, enabling the computation of the $k/s_{\lambda,mixture}$ for custom mixtures of these colorants. Consequently, this can predict the reflection and, ultimately, the resultant color of these custom blends [50].

$$X_{m,1} = -C_1 \tag{4a}$$

$$X_{m,2} = -C_2 \tag{4b}$$

$$X_{m,3} = -C_3 \tag{4c}$$

$$X_{m,4} = -C_4 \tag{4d}$$

$$X_{m,5} = -C_1(K/S)_{mix} \tag{4e}$$

$$X_{m,6} = -C_2(K/S)_{mix} \tag{4f}$$

$$X_{m,7} = -C_3(K/S)_{mix} \tag{4g}$$

$$X_{m,8} = -C_4(K/S)_{mix} \tag{4h}$$

$$KSCOEFS = \begin{bmatrix} X_{1,1} & \cdots & X_{1,8} \\ \vdots & \ddots & \vdots \\ X_{m,1} & \cdots & X_{m,n} \\ 1 & \ldots & 1 \end{bmatrix} \tag{5}$$

$$KANDS=\begin{bmatrix}K_1\\K_2\\K_3\\K_4\\S_1\\S_2\\S_3\\S_4\end{bmatrix}=\left(KSCOEFS^{'}KSCOEFS\right)^{-1}KSCOEFS^{'}OBS \quad (6)$$

3. Methods and instruments

In the following sections, the color reproduction process will be explored through experimental procedures. The Kubelka-Munk [36] methodology will be examined to establish initial color proportions. The objective function, central to quality assessment, will be discussed alongside distinct error metrics. Optimization methods, boundaries for proportion refinement, and interpolation for reflectance data standardization will be detailed.

3.1. Experiment

In this study, eight different samples made from PLA were used from recycled 3D printing scrap. The samples are each identified by their color hex code, which is a means of representing colors in a format that computers can read and display. These samples included various colors: cyan (HEX Code- #0066D9), magenta (HEX Code- #F2306E), black (HEX Code- #080A0D), navy blue (HEX Code- #003776), green (HEX Code- #06924D), cream (HEX Code- #E5C8A2), purple (HEX Code- #6C47B2), and red (HEX Code- #E0191E). All samples were created using filaments from Polymaker [51]. First, these previously 3D printed samples were shredded using a shredder (Filabot Reclaimer 220VAC [52]). 12 mm diameter shredded plastic was transferred to the granulator to be reduced in size less than 10 mm. Then, the shredded plastics were transformed into rectangular prisms shapes through compression molding (Figure 2). Compression molding provides a simple method to form thermoplastic regrind into a solid with a consistent flat surface for subsequent spectroscopy. This process relies on the ability of thermoplastics to flow above their glass transition temperature to reform the regrind into a homogenous solid. To accomplish this, the plastic must first be loaded into a prepared mold and softened under elevated temperatures before applying an external pressure to force the melted plastic to adopt the internal shape of the mold. These molds must consist of a cavity matching the desired final plastic form and some form of a plug or punch to force the plastic into this cavity (Figure 3) [53].

To produce the desired spectroscopy blanks for this study, the mold consisted of 12 equally sized rectangular pockets measuring 1/2 inch × 1 inch and 1 inch in depth. Each pocket was associated with a plug with a slightly undersized footprint and a 1/2 inch height. This mold allowed a single compression process to produce an array of PETG or PLA color samples simultaneously at a reduced testing and cycle time. To complement this mold, an upper and lower “lid” of 1/8 inch aluminum was used to seal the plastic inside during compression molding while simultaneously allowing trapped air to escape. To process this mold, the open-source scientific press [54] was used which provided a 12 inch × 12 inch

upper and lower platen to heat the aluminum mold and melt the enclosed plastic charge. Once heated, the incorporated 4-ton hydraulic bottle jack was actuated to form the plastic into the mold.

To prepare the mold, the colors of interest were first cut from waste PLA 3D prints into grounds just small enough to fit within the 1/2 inch × 1/2 inch × 1 inch pocket or shredded into smaller grain sizes for ease of mold loading [53]. Based on the volume of the mold and the density of the thermoplastic of interest, the required weight of plastic necessary to occupy the mold cavity was calculated and weighed out for each color. Due to the air gaps between plastic grains, the small footprint being loaded, and the depth of the cavity, the mold had to be filled and compressed in stages (Figure 3).

Figure 2. Compressed waste plastic samples: Top row (left to right) - red, blue, black, gray; Bottom row (left to right) - dark purple, purple, white, and cream.

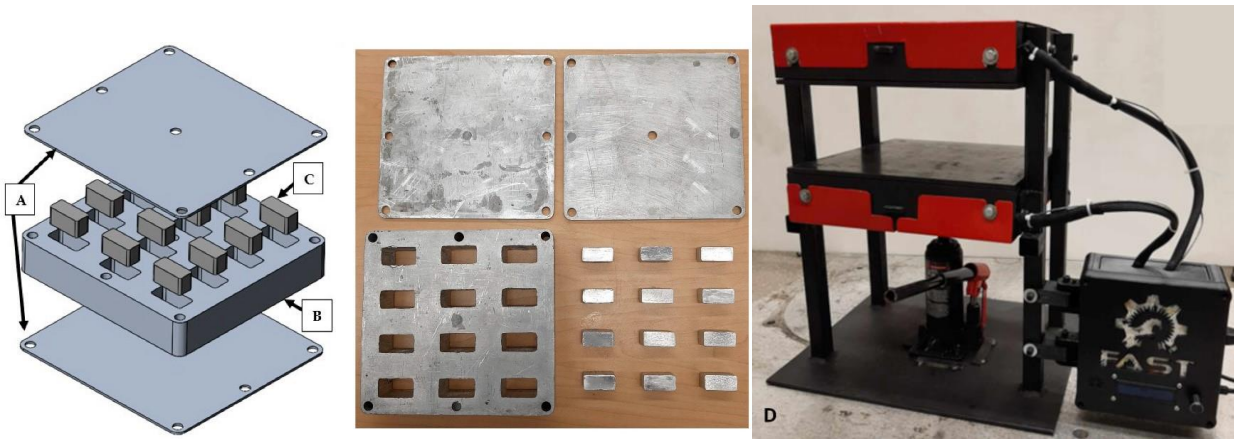

Figure 3. Laser-cut aluminum mold used for sample production [53]. **(A)** Mold Lid X2; **(B)** ASTM D695 Mold; **(C)** Mold Plug X12; **(D)** the open-source scientific hot press.

As such, the cavity was nearly filled to the top surface of the mold and, once the hot press had reached the melting temperature of the plastic, the mold was placed between the two heated platens. The plastic was allowed to soften for approximately 5 minutes, before it was removed and the partially loaded cavities manually compressed (using clean pliers, a screwdriver, or similar handheld tool). The mold was topped up, returned to the hot press, and the process repeated until all weighed plastic was used. Once complete, a plug was placed inside each pocket, the remaining aluminum lid placed on top, and

the entire mold returned to the hot press. At this point, the hydraulic bottle jack was actuated, and the pressure increases until the mold was sealed. The system can apply pressures up to 0.38 MPa. The fully loaded mold was allowed to sit for up to 10 minutes to ensure the plastic had settled to form a homogenous brick, at which point the hot press was turned off. The samples were cooled under pressure to avoid warping before being ejected from the mold. Upon part removal, all flash was trimmed to prepare the sample for spectroscopy. It is important to note that all mold components were cleaned and scraped using acetone in between sample production to prevent color contamination from previous trials.

Spectroscopy was used to obtain the reflectance spectrum of each of the samples [55]. The measurements produce a dataset of percent absorption (%) for wavelengths along the visible spectrum. The absorption measurement used an Ocean Insight HL-2000-LL light source, QR400-7- VIS-NIR fiber optic probe [56] and SR4 UV-VIS spectrometer. A reflection probe holder was 3-D printed (Figure 4) for the purpose of maintaining a constant distance and angle between the sample and probe (5cm and 90 degrees between surface and probe). The probe was positioned at 90 degrees to the sample as recommended by the spectrometer manufacturer. Signal to noise ratio is reduced by keeping the sample as close to the probe as possible. After experimentation, 5 cm was determined to be a reasonable distance to maintain signal integrity and was used here. Ocean Insight software requires a reference sample reading and background reading before sample measurements can be taken [55]. A pure white PETG sample was used as the reference sample to maintain material consistency while only altering the color profile. The background reading was taken by placing the probe directly on a matte black surface while the light source was off. For samples, reflectance scans to average were set to 25 and boxcar width set to 25 for a total dwell time of 4 seconds. Three measurements were taken on different areas of each of the samples. Spectral data for each sample was obtained from the spectrometer, with reflectance values ranging from 0 to 100. The data, however, needs to be standardized with an even step size and reported in percentage format so it was exported into a spreadsheet and subsequent data analysis was performed using Python [37] using the whole wavelength interpolation code. After determining the color proportions, the samples were extruded using a ProtoCycler+ [57] recyclebot and molded one more into uniform cube shapes using the hot press to facilitate thorough blending. The reflectance measurements were then repeated.

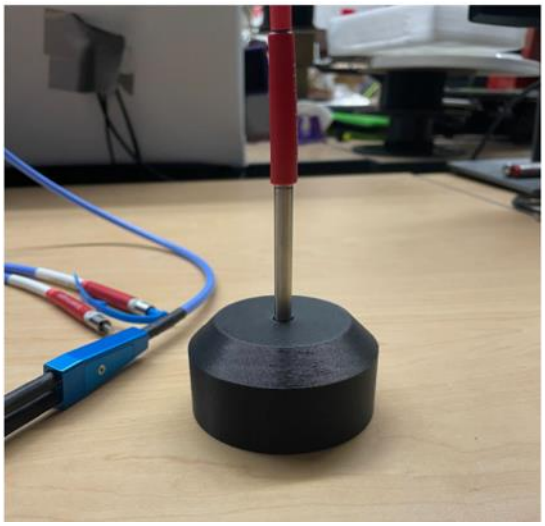

Figure 4. 3-D printed probe holder.

As a proof-of-concept the specific color, Western University purple, was used. It is represented by the hex color code #4F2683, and is characterized by RGB values of (79, 38, 131) [58]. Although purple is typically composed of cyan, magenta, and black (CMYK: 40, 71, 0, 49) [59], its exact composition may vary depending on the different shades and available colors. To ensure a precise match with the target sample, adjustments might be needed, such as the addition of white, black, or various shades of either blue or red, depending on the specific shade of purple. The case study demonstrates how to get any specific color. The novel color composed of waste plastic scraps is then extruded into filament to recreate the Western Purple.

3.2. Kubelka-Munk

Once the initial proportions are determined through the Kubelka–Munk methodology, an objective function is formulated, and initial guesses are defined for optimization through distinct optimization methods. The objective function [35], is used to assess and quantify the quality of color reproduction based on specified proportions of color components available. It operates by calculating an objective value that combines two fundamental error metrics: the RMS error and the ΔE error. The RMS error quantifies the overall disparity between the color predicted by the model and the target color. This is achieved by computing the square root of the mean of squared differences between corresponding color components. Simultaneously, the ΔE error measures perceptual differences between the predicted and target colors by transforming both into the LAB color space. This transformation considers LAB components L, a, and b and then measures CIE2000, enabling a comprehensive evaluation of perceptual differences. The objective function was independently formulated with the primary objective of minimizing both errors through experimentation with various divisions. The adjustments for color difference demonstrated minimal impact compared to RMS, indicating a greater emphasis on replicating the curves. Consequently, the objective function combines these error metrics, assigning different weights to each (0.9 for RMS and 0.1 for ΔE), to provide a unified measure of color reproduction quality. Thus, the algorithm targets the lowest RMS and ΔE simultaneously. Among the others, this algorithm was the optimum meaning that it neither had the highest or lowest of each evaluation metric.

3.3. OS software

This section discusses the experimental steps, including data interpolation, initial color proportion estimation using Kubelka-Munk theory, and the application of three optimization methods. These methods are compared based on RMS error and color difference (ΔE) values, contributing to the exploration of color optimization in waste plastic transformation [35].

3.3.1. Interpolation

To enhance data quality and achieve a uniform 10-nanometer step size for reflectance data, an interpolation function was employed for each color's reflectance data. This function confines the wavelength range between 400 and 700 nanometers. The number of data points generated is determined by dividing the difference between the upper and lower bounds by 10, ensuring the desired 10-nanometer intervals. For data points for a function f(x) at X_1, X_2, ..., X_n, to find the value of f(x) for a point $x_{i-1} < x < x_i$, it is crucial to note that if the difference between xi and x_i, x_{i-1}, denoted as a_i,

is relatively small, linear interpolation is accurate enough, especially when the function is continuous [60]. This approach can, however, introduce errors when the value change sharply. Figure 5 presents the reflectance data both before and after undergoing interpolation for three of the samples. As shown, interpolated curves exhibit a notably smoother appearance in comparison to curves before the operation.

Figure 6 shows the available colors used in the experiments for the test after the interpolation.

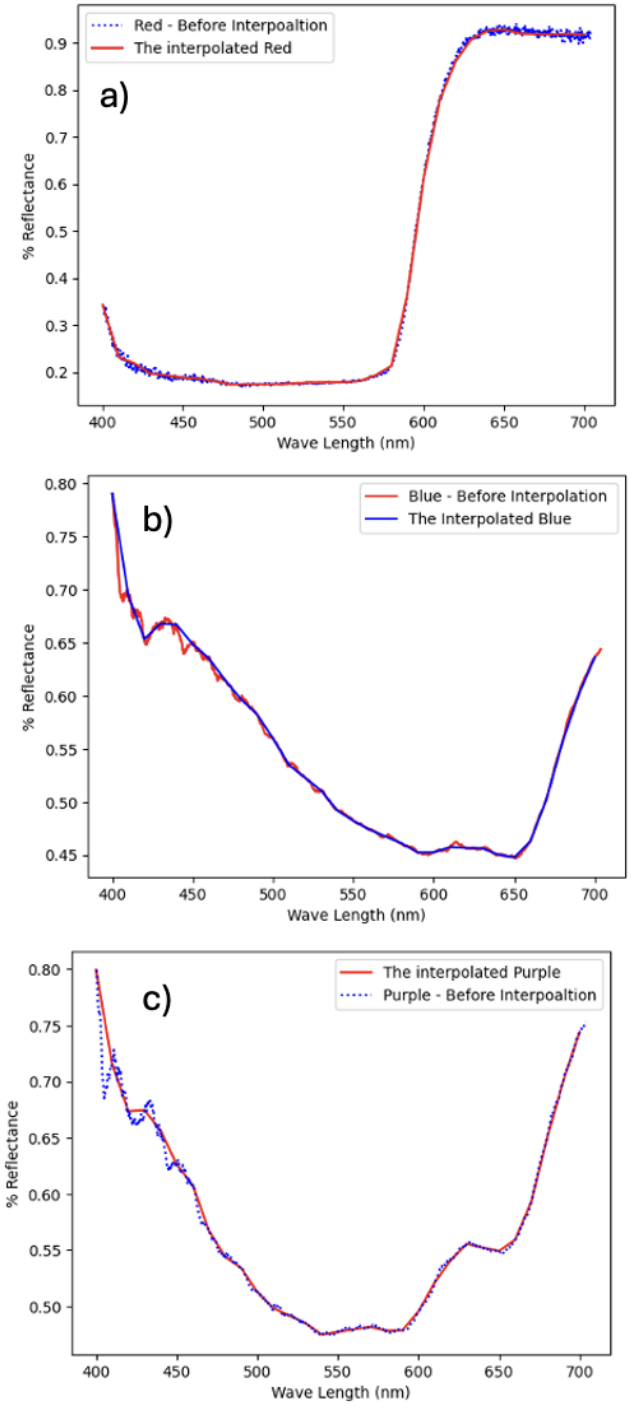

Figure 5. Reflectance curve for the colors red, pre- and post-interpolation for **a)** Red; **b)** Blue; **c)** Purple samples.

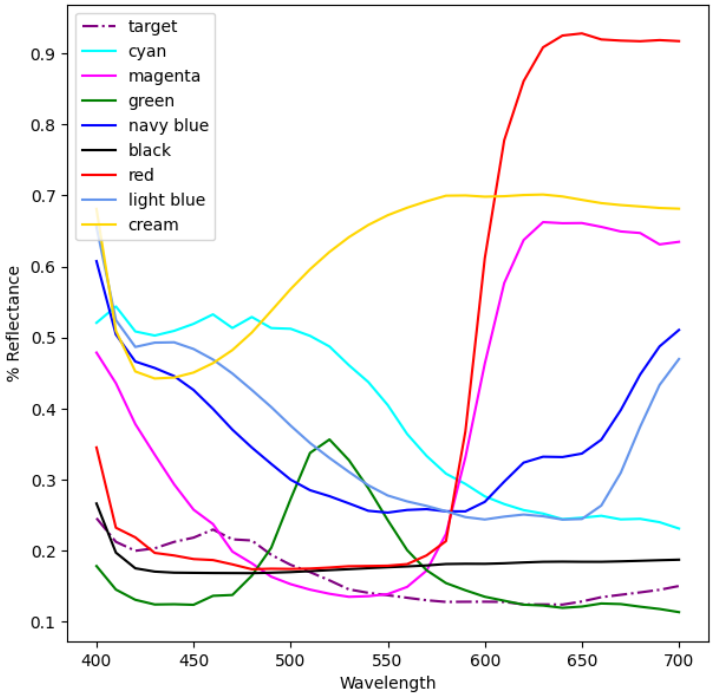

Figure 6. Reflectance curve for the recycled colors after the interpolation.

3.3.2. Functions

Subsequently, the Kubelka-Munk theory was applied to derive initial estimations for each color's proportions as the starting point for the optimization process. The Walowit [48] approach for Kubelka-Munk theory was used to obtain the starting points for the mixtures. To perform this for each sample, a tint ladder was established, where the colors with white in six different concentration ratios: 0:100 (full white), 20:80, 40:60, 60:40, 80:20, and 100:0 (mass tone). In the optimization phase, all three methods were employed, and their results were compared to identify the one with the lowest RMS error and color difference ΔE values. The procedures for all optimization methods remained consistent and included the following steps. Initially, the dataset with a 10-nanometer step size was imported from a spreadsheet, and each color's data was separated into individual columns. A function named 'ref2lab' was employed for the conversion of reflectance data into the CIELAB color space, which is essential for achieving consistent and precise color reproduction [61]. CIELAB, also known as CIE L*a*b*, represents a three-dimensional, device-independent color space, facilitating the accurate measurement and comparison of all discernible colors through three color values [62]. Within this color space, numerical variations in values are indicative of the perceptible differences in color as perceived by humans. Utilizing the L*a*b* chart values, precise calculations enable the quantification of the difference between specific colors, known as delta (Δ) [63]. This calculation is done through 'cal_delta_e' function. To measure the RMS error, a 'weighted_rms' function was defined to return the root mean square between the weighted rms of the reconstructed and the actual curve. The blue region of the spectrum and the red region needed more attention compared to the mid-spectrum. Consequently, the proportion of the contributing colors are weighted during the optimization through the RMS.

Next, a function named 'objective function' was used for evaluating the quality of a color matching process. Input proportions are multiplied by their corresponding curve, and a predicted color was

determined through weighted combinations of distinct color components. Subsequently, the RMS error and ΔE functions are called. The evaluation metrics were then harmonized by the objective function, with a 90% emphasis on the RMS error and a 10% emphasis on the ΔE error because it is important to reconstruct the same reflectance curve. This resulted in a single assessment value for the optimization and color matching procedures.

3.3.3. Optimization methods

The boundaries for each proportion are determined and the initial estimates obtained from the Kubelka-Munk method are employed. In this process, all proportions are constrained within a range from 0 to 1. Subsequently, each of the selected optimization methods is individually applied to the objective function and the optimized proportions are utilized to reconstruct the new reflectance curve. A comparison is made between the reconstructed curve and the actual color's reflectance data using RMS and ΔE as evaluation criteria.

All optimization methods are from the SciPy [38] library and employ the 'minimize' function, offering three different minimization methods. These methods are capable of working with bounds and avoid returning negative quantities. In this study, returning negative values is physically impossible.

The first method is 'Nelder-Mead', which utilizes the Simplex algorithm and is robust in various applications [39]. When reliable numerical derivatives are available, however, algorithms using first and/or second derivatives information might be preferred for their generally better performance [40]. The Nelder-Mead algorithm effectively minimized the objective function in the study [64], achieving small mean differences in profile dose in depth-dose in phase space optimization highlighting the algorithm's simplicity and faster initial convergence.

The L-BFGS-B (limited-memory Broyden–Fletcher–Goldfarb–Shanno algorithm) method employs the L-BFGS-B algorithm to perform minimization with bound constraints [65,66].

SLSQP, sequential least quadratic programming, is valuable for process optimization but often requires many function evaluations [67].The core concept of SLQP is to create a simplified quadratic model during each iteration at X_k. This model is utilized to update X_k with the step S_k, and the approach can be readily expanded to incorporate inequality constraints [68].

3.3.4. Validation tests

Three colors were selected to perform a validation test on the method to evaluate the real-world applicability of the optimized algorithm. This was employed to reconstruct: 1) Western University purple, 2) Navy Blue [51] and 3) the pink petals of the wildflower bouquet LEGO set [69]. To verify the efficiency of the selected algorithms, all three algorithms were applied to reconstruct the three colors. The aim was to determine the best method among the proposed algorithms by finding the one that produces the least amount of error in terms of accuracy, as defined by the objective function. This experiment utilized the primary colors associated with subtractive mixing (Figure 1), as well as additional colors. There may be instances, however, where not all the necessary colors are available. Consequently, this study simulated this situation by reconstructing the case study target colors using only four colors.

Figures 7–9 show a summary of the whole process.

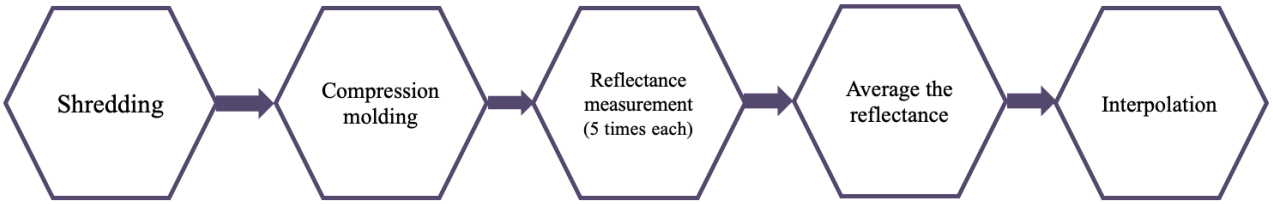

Figure 7. A summary of data and sample preparations.

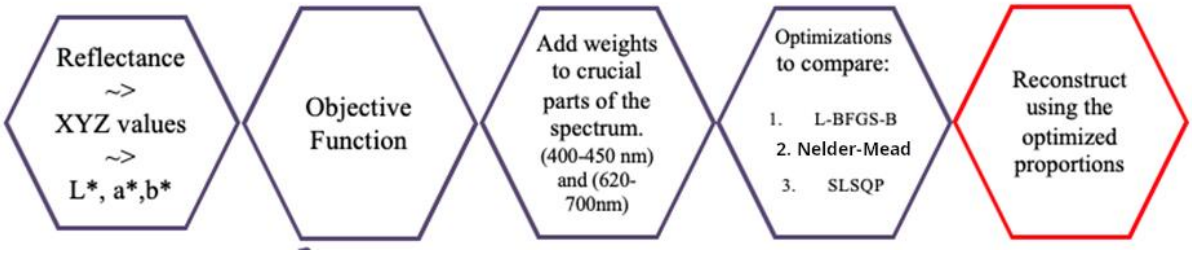

Figure 8. A summary of how the software works.

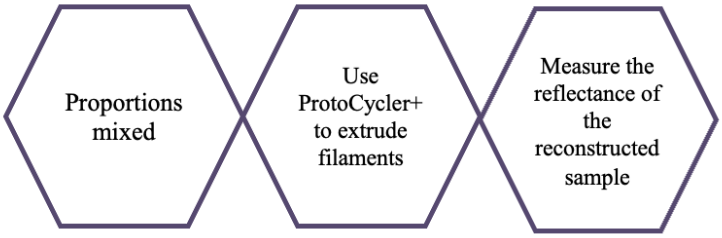

Figure 9. A summary of steps for reproduction of the colors with the proportions.

4. Results and discussions

Table 1 indicates the proportion of each sample output by the software to reconstruct the Western University purple. Table 2 presents the RMS and ΔE errors associated with each optimization technique in reproducing the Western Purple and Navy-blue color. Figure 10 and Figure 11 present reconstructed reflectance data alongside the target reflectance for all three algorithms, represented by the Western University purple and Navy-Blue samples, for comparison.

Table 1. Ratios of individual colors to reconstruct Western Purple in various optimization methods with constraints ranging from 0 to 1.

Color Method	cyan	magenta	green	navy blue	black	red	light blue	cream
L-BFGS-B	2×10^{-4}	2.08×10^{-1}	0	8.65×10^{-2}	1.04×10^{-1}	2.7×10^{-3}	6.68×10^{-1}	0
Nelder-Mead	1.2×10^{-3}	2.23×10^{-1}	2.1×10^{-1}	3.9×10^{-2}	2.9×10^{-3}	3.3×10^{-1}	7.31×10^{-1}	1×10^{-4}
SLSQP	0.37	0.11	0.03	0.14	0.18	0.13	0.24	0.29

Table 2. RMS and Delta E values for various optimization methods to reconstruct Western Purple and Navy Blue.

	Western Purple		**Navy Blue**	
Optimization	ΔE	RMS	ΔE	RMS
L-BFSG-B[6]	0.665	0.0396	2.874	0.0217
Nelder - Mead	3×10^{-5}	0.0241	1.2×10^{-4}	0.0386
SLSQP	8.4143	0.0821	3.628	0.0318

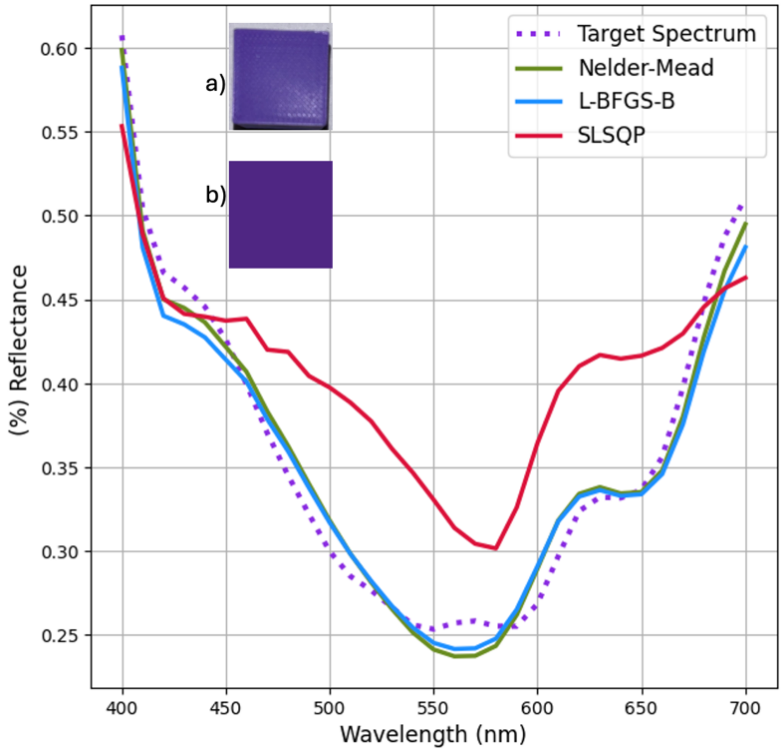

Figure 10. Reconstruction of the Western Purple using three optimization algorithms. Insets: **a)** the reconstructed color using the plastics and **b)** the original purple (target) used to reproduce.

Upon analyzing the outcomes and applying a custom function, it becomes evident that, for these colors, the Nelder-Mead minimization method in the SciPy library stands out as the preferable choice, despite not having the lowest values in both accuracy measures. To illustrate how this could be used, Figure 12 presents a comparison of the reconstructed curve with the actual measured sample for the Lego pink color. The DELTA E value recorded for this sample is 1.5×10^{-4}, and the RMS error is 0.0234, indicating minor discrepancies as clearly shown in Figure 12.

Next the potential source colors were limited to better illustrate resource constrained settings. As a result of limiting the number of colors used to reconstruct the three case study colors, the accuracy of the outcomes diminished due to the reduced spectral data available for reconstruction across various parts of the spectrum. Nevertheless, it is feasible to achieve a nearly accurate result, but the accuracy improves as the number of source colors increases. Figures 13 and 14 show the reconstructed spectral curve of Western Purple and Navy Blue, respectively using only four samples. Table 3 indicates the

color difference and the RMS for these samples. The findings indicate that the Nelder-Mead algorithm remains the optimal choice even when limited to using only four samples.

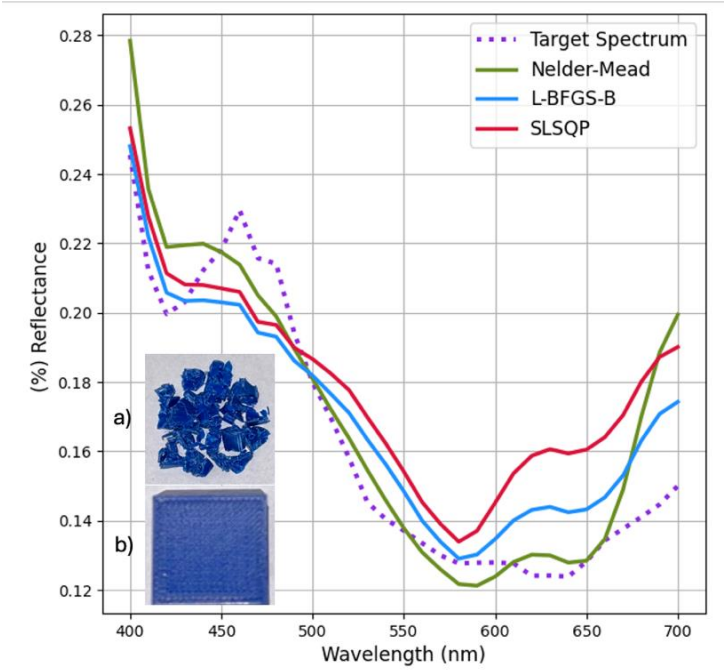

Figure 11. Reconstruction of the Navy Blue using three optimization algorithms. Insets: **a)** the original color used to reproduce and **b)** the reconstructed color using the plastics.

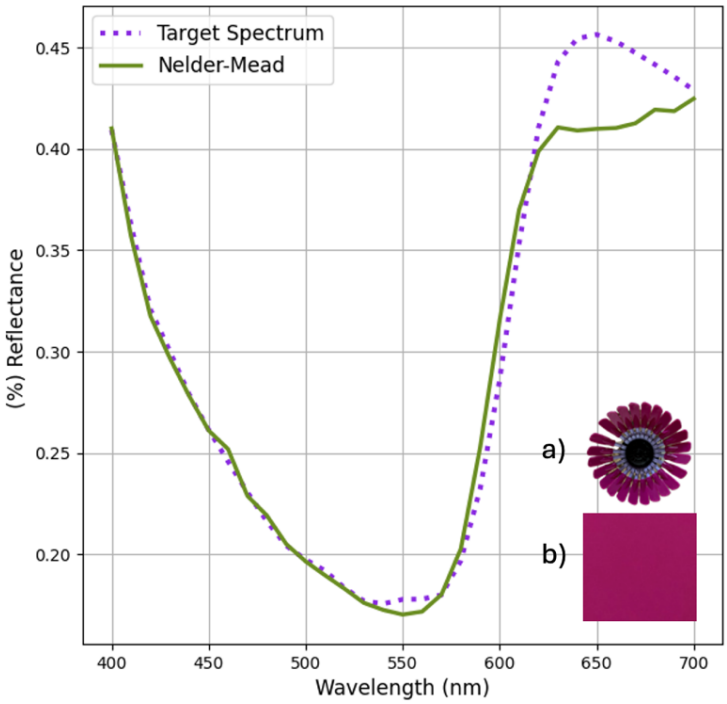

Figure 12. Reconstruction of the LEGO pink using Nelder-Mead optimization algorithm. Insets: **a)** the petals of the flower used to reproduce and **b)** the reconstructed color using the recycled plastics.

A recommendation for industries is to compile a color palette encompassing all previously printed samples and record their reflectance data to develop a comprehensive dataset. This approach enhances the accuracy of reconstructions, as a larger data set provides more data for analysis. It is, however, important to consider the infill of the prints, as prints with low infill may not yield high-quality reflectance data. Therefore, it is advisable to ensure the infill is adequate before proceeding with measurements.

Given the consistent objective function and initial guess across all optimization methods, the Nelder-Mead method stood out as the most efficient approach among the three libraries and eight combinations tested. It achieved the optimal level of error for both metrics and demonstrated exceptional computational efficiency and speed. Using this method coupled to DRAM will add to the literature moving forwards in sustainable manufacturing [70] and industry 4.0 [71].

Table 3. RMS and Delta E values for various optimization methods to reconstruct Western Purple and Navy Blue with 4 colors.

	Western Purple		**Navy Blue**	
Optimization	ΔE	RMS	ΔE	RMS
L-BFSG-B[6]	6.5497	0.1408	4.880	0.0251
Nelder–Mead	2.8239	0.1541	2.988	0.0292
SLSQP	6.6889	0.1884	4.1529	0.0312

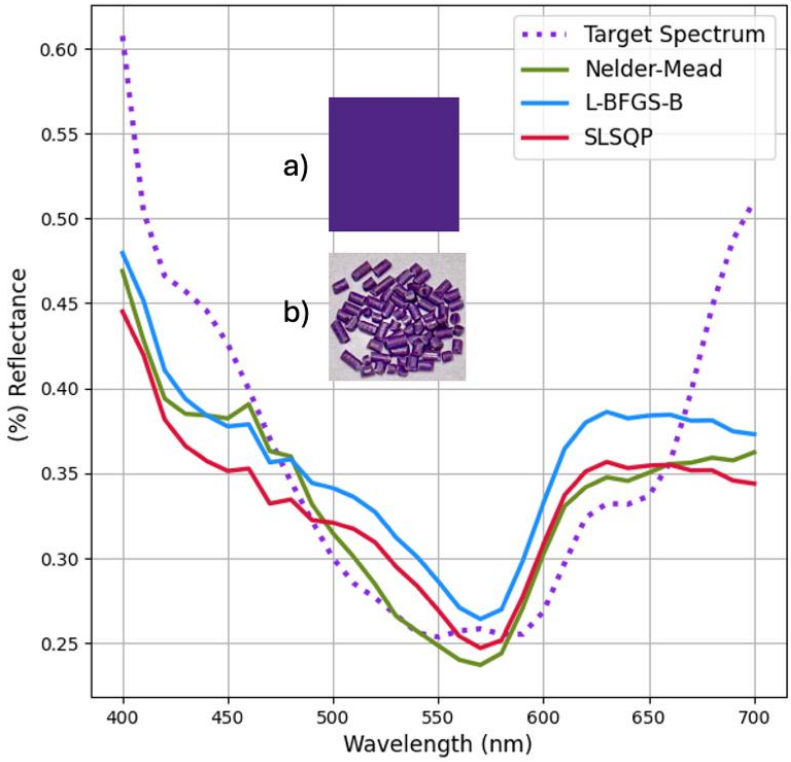

Figure 13. Reconstruction of the Western Purple color using four colors (cyan, magenta, green, and black). The optimization methods employed are Nelder-Mead, L-BFGS-B, and SLSQP. Insets: **a)** the original purple used to reproduce and **b)** the reconstructed color using the mixture of recycled plastics.

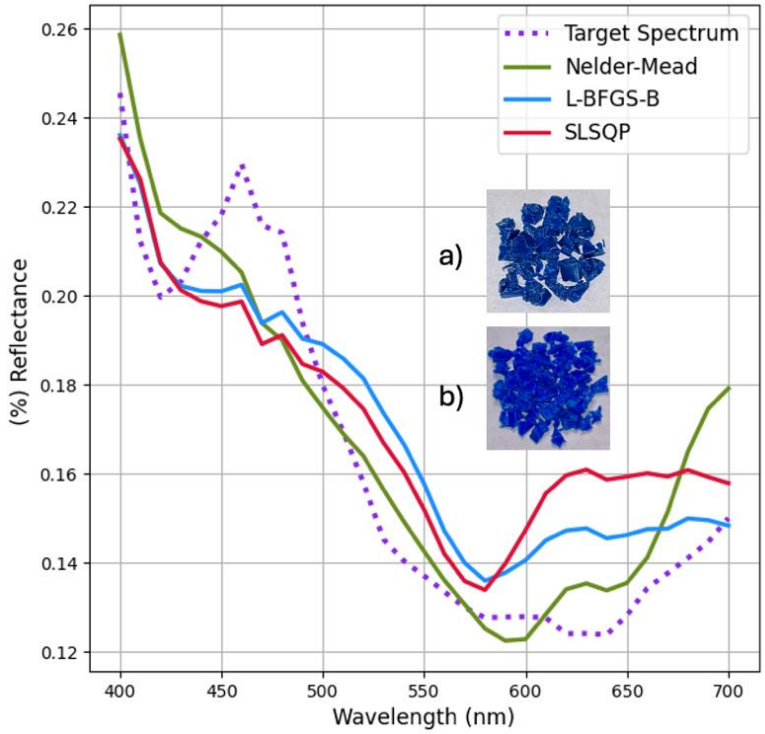

Figure 14. Reconstruction of the Navy-Blue color using four colors (cyan, magenta, green, and black). The optimization methods employed are Nelder-Mead, L-BFGS-B, and SLSQP. Insets: **a)** the original purple used to reproduce and **b)** the reconstructed color using the recycled plastics.

4.1. Limitations

When employing waste plastic for reproduction of specific colors for 3-D printing, several challenges may arise. One of the primary challenges involves the potential variation in the spectral reproduction equation, contingent upon the availability and intensity of colors. For example, to replicate the color purple, the necessity of blue and red is apparent. For example, if the available blue color differs in terms of its shade or intensity, it is crucial to measure the spectra again and begin the optimization process afresh to determine the revised proportions. In some cases, achieving an exact match to the target color may be unattainable due to the absence of the necessary initial colors for reconstruction. For instance, in this study utilizing a green sample for spectral data reproduction can contribute to error reduction, as it involves measuring L*, a*, and b* values through RGB values, however, even in the absence of the green color, both errors remained minimal.

The results here show the utility of the approach for three colors, future work could evaluate a broader range of colors to ensure that there were no issues from this approach to practical applications. For example, blending plastics with diverse materials necessitates the inclusion of additional substances to ensure their suitability for 3-D printing by imparting dependable physical properties [72]. This may cause challenges with measuring the color for the algorithm.

In addition, the prudent practice of preparing and documenting the spectral data of available base samples at the outset facilitates color measurement and decision-making. This pre-existing database can expedite the process, particularly in cases where waste samples lack information or possess unclear material properties. Moreover, it helps with the time-consuming necessity of grinding, molding, and

individually measuring each sample as needed. It is recommended that manufacturers make this data available to their customers to help encourage recycling of their materials.

It should be noted that even for a given color if manufacturers make it in a different way (e.g., different additives) and the color is truly different this method will work. This method would get a spectra for each filament/plastic from a given manufacturer. Then this value would be used to do the color mixing. The ratio that the software outputs may be different for different manufacturers if the color of their filaments differ. In addition, surface roughness can impact the refraction/reflection of light and thus impact color. This method does not completely control this effect. The way the colors are measured are all with a relatively flat low roughness surface from the press—but when printed these colors will be impacted by surface roughness. Future work is needed in this area.

The method developed here worked, and could readily be applied to schools, libraries, community centers, makerspaces and fab labs because of the concentration of 3D printing waste, however it may be challenging for individual users. Although open-source spectrometers [73–76] exist, they are not readily available and still may be cost prohibitive for some families. Utilizing online tools for acquiring RGB values simplifies the process of deriving XYZ and subsequently CIELAB values of a color and could represent a limited solution to the problem. This method does not capture the spectral data, which contains critical information about a color's saturation. In cases where only the target sample's CIELAB values are available, the evaluation of color accuracy in optimization methods is confined to using color difference metrics. To validate this assertion, a color picker tool named Colorzilla [77] was used as a Google Chrome extension to ascertain the RGB values from Western University's website. Attempting to reconstruct the color without spectral data resulted in a color difference of 12.097, indicating a substantial deviation from the actual color. The three optimizations functions all worked, but future work could also investigate the other minimization options available in the SciPy [38] library.

A Delta E value of 12.097 indicates a noticeable color difference between two colors. The Delta E formula is a metric for understanding how the human eye perceives color difference. Therefore, a ΔE value of 12.097 means that the color difference is very apparent, and the two colors can be clearly distinguished from each other even without close examination. This level of difference is typically considered unacceptable in contexts where color matching is critical, such as in textile manufacturing, paint production, and digital media. The difference achieved by the SpecOptiBlend for all the three samples using the optimized algorithm, reached amounts close to zero. This indicated the closeness of the results to the actual colors.

4.2. Future work

A preference for employing a standardized white reference for reflectance measurement is suggested. In subsequent research, the inclusion of all fundamental colors, including cyan, magenta, yellow, black, red, green, and blue, is deemed advantageous, enhancing the potential for color reproduction. Furthermore, leveraging online color pickers enables the extraction of RGB values, facilitating their conversion to CIELAB. A comparative analysis can then be conducted between these CIELAB values and those resulting from the amalgamation of available colors with optimized proportions.

The excellent results of this study demonstrate that custom colored AM feedstock can be made from waste plastic only during DRAM to create a higher value product by employing the open source SpecOptiBlend software released and demonstrated here. In the most eco-friendly form of DRAM,

prosumers create their own products using 3-D printing materials in their homes. This approach aims to minimize the energy and greenhouse gas emissions associated with product manufacturing [22]. DRAM is a versatile technology with global applicability, even in regions where recycling services are lacking, and in extreme cases, where electricity availability may be limited [8,78]. The latter of which can be overcome by the use of solar photovoltaic powered recyclebots [79,80] and 3-D printers [81–84]. DRAM holds the potential to influence global value chains, particularly as 3-D printing and localized manufacturing trends continue to reshape these chains. Lastly, it should be noted, a more effective method for DRAM has been introduced, which involves the direct extrusion of recycled plastic waste in 3-D printing. This technique is known as fused granular fabrication (FGF) or fused particle fabrication (FPF) and has been demonstrated for a wide range of waste plastics [28,29,84–86]. In essence, it improves the efficiency of the DRAM process because the material only needs to be melted once. While it is feasible to implement FPF/FGF on desktop printers, this approach is more complex and better suited for larger plastic items. When considering greenhouse gas (GHG) emissions, substantial plastic products like furniture or building components, with extended lifecycles, serve as long-term carbon storage solutions and have the capacity to consume significant amounts of plastic waste [87]. Future work is needed to determine if the color customization approach demonstrated here with FFF can be adapted to FPF/FGF. There are other areas of future work. First, as it has been shown that color impacts mechanical properties [33], future work is needed to quantify the impacts of color targeting on the mechanical properties of the different waste plastic feedstocks. In addition, DRAM has been demonstrated for a wide array of waste plastics in addition to PLA/PETG and should be evaluated for SpecOptiBlend color picking. These plastics include: high-density polyethylene (HDPE) [87–89], low-density polyethylene (LDPE) [90], acrylonitrile butadiene styrene (ABS) [78,83,84,87], polypropylene (PP) and polystyrene (PS) [88], thermoplastic polyurethane (TPU) [91], polyethylene terephthalate (PET) [92,93], and polycarbonate (PC) [94]. Finally, in DRAM one of the means of changing/improving properties of a material are with the use of additives such as waste wood [95], fiber [96,97], glass [98,99], carbon fiber [100], and blends [101,102]. The impacts of these additives on color optimization also need to be evaluated.

5. Conclusions

The open-source SpecOptiBlend software has shown remarkable effectiveness in producing customized colors from recycled plastics, addressing the prevalent issue of color inconsistency in recycling processes. This enhancement marks a significant step forward in integrating circular economy principles into 3D printing practices. A range of sophisticated optimization algorithms—Nelder–Mead, L-BFGS-B, and SLSQP—enabled the matching of colors using mixed waste plastics. Among these, the Nelder-Mead method stood out, striking an optimal balance between the precision of color differences (ΔE) and root mean square error (RMS), essential for producing high-quality colors.

This research has provided a free tool that will now enable prosumers to convert their plastic waste into specific custom colors to enable DRAM. Future work could provide integration of online color identification tools to further refine color matching accuracy. Additionally, extending the range of recyclable plastics and incorporating different additives could improve the mechanical properties and fidelity of colors in recycled products.

Acknowledgments

This research was supported by Thompson Endowment and the Natural Sciences and Engineering Research Council of Canada (NSERC).

Authors' contribution

Conceptualization, J.M.P.; methodology, K.A., J.G., M.W. and J.M.P.; software, K.A., J.G., M.W. and J.M.P.; validation, K.A., J.G., M.W. and J.M.P.; formal analysis, K.A., J.G., M.W. and J.M.P.; investigation, K.A., J.G. and M.W.; resources, J.M.P.; data curation, K.A., J.G., M.W. and J.M.P.; writing—original draft preparation, K.A., J.G., M.W. and J.M.P.; writing—review and editing, K.A., J.G., M.W. and J.M.P.; visualization, K.A., J.G. and M.W.; supervision, J.M.P.; project administration, J.M.P.; funding acquisition, J.M.P. All authors have read and agreed to the published version of the manuscript.

Conflicts of interests

The authors declare no conflict of interest.

References

[1] Sells E, Bailard S, Smith Z, Bowyer A, Olliver V. RepRap: the replicating rapid prototyper: maximizing customizability by breeding the means of production. In *Handbook of Research in Mass Customization and Personalization*. Singapore: World Scientific, 2009. pp. 568–580.

[2] Jones R, Haufe P, Sells E, Iravani P, Olliver V, *et al.* RepRap – the replicating rapid prototyper. *Robotica* 2011, 29(1):177–191.

[3] Bowyer A. 3D printing and humanity's first imperfect replicator. *3D Print. Addit. Manuf.* 2014, 1(1):4–5.

[4] Rundle GA. Revolution in the Making: 3D Printing. In *Robots and the Future*. South Melbourne: Affirm Press, 2014.

[5] Kostakis V, Papachristou M. Commons-based peer production and digital fabrication: the case of a RepRap-based, Lego-built 3D printing-milling machine. *Telemat. Inform.* 2014, 31(3):434–443.

[6] Halassi S, Semeijn J, Kiratli N. From consumer to prosumer: a supply chain revolution in 3D printing. *Int. J. Phys. Distrib. Logist. Manag.* 2018, 49(2):200–216.

[7] Yoo B, Ko H, Chun S. Prosumption perspectives on additive manufacturing: reconfiguration of consumer products with 3D printing. *Rapid Prototyping J.* 2016, 22(4):691–705.

[8] Petersen EE, Pearce J. Emergence of Home Manufacturing in the Developed World: Return on Investment for Open-Source 3-D Printers. *Technologies* 2017, 5(1):7.

[9] Pearce JM. Economic savings for scientific free and open source technology: a review. *HardwareX* 2020, 8:e00139.

[10] Ventola CL. Medical applications for 3D printing: current and projected uses. *Pharmacol. Ther.* 2014, 39(10):704–711.

[11] Pearce JM. Distributed manufacturing of open source medical hardware for pandemics. *J. Manuf. Mater. Process.* 2020, 4(2):49.

[12] Di Pietro L, Fortunato GM, Botte E, Ahluwalia A, De Maria C. Open-source medical devices as tools for teaching design, standards and regulations of medical technologies. In *Engineering Open-Source Medical Devices: A Reliable Approach for Safe, Sustainable and Accessible Healthcare*. Cham: Springer International Publishing, 2022. pp. 219–242.

[13] Hoppe M, Burger M, Schmidt A, Kosch T. DronOS: a flexible open-source prototyping framework for interactive drone routines. In *Proceedings of the 18th International Conference on Mobile and Ubiquitous Multimedia*, New York, USA, November 26, 2019, pp. 1–7.

[14] Tipker GG, Golub M, Dube TC, Zhang J. Integration of 3-D Printed Drone Project in General Engineering Curriculum. In *2019 ASEE Annual Conference & Exposition*, Tampa, USA, June 16–19, 2019.

[15] Byard DJ, Woern AL, Oakley RB, Fiedler MJ, Snabes SL, *et al.* Green fab lab applications of large-area waste polymer-based additive manufacturing. *Addit. Manuf.* 2019, 27:515–525.

[16] Coakley MF, Hurt DE, Weber N, Mtingwa M, Fincher EC, *et al.* The NIH 3D Print Exchange: A Public Resource for Bioscientific and Biomedical 3D Prints. *3D Print. Addit. Manuf.* 2014, 1(3):137–140.

[17] Coakley M, Hurt DE. 3D Printing in the Laboratory: Maximize Time and Funds with Customized and Open-Source Labware. *J Lab Autom.* 2016, 21(4):489–495.

[18] Horton J, Xiong JA. A Comparison of Three Emerging Online Government 3D Printing Resources: NASA 3D Resources, Smithsonian X3D, and the NIH 3D Print Exchange. 2016, Available: https://annurev.publisher.ingentaconnect.com/contentone/annurev/tca/2016/00000018/00000002/art00004 (accessed on 23 October 2023).

[19] Petersen EE, Kidd RW, Pearce JM. Impact of DIY Home Manufacturing with 3D Printing on the Toy and Game Market. *Technologies* 2017, 5(3):45.

[20] Gallup N, Pearce JM. The Economics of Classroom 3-D Printing of Open-Source Digital Designs of Learning Aids. *Designs* 2020, 4(4):50.

[21] Gallup N, Bow JK, Pearce JM. Economic Potential for Distributed Manufacturing of Adaptive Aids for Arthritis Patients in the U.S. *Geriatrics* 2018, 3(4):89.

[22] Pearce J, Qian J-Y. Economic Impact of DIY Home Manufacturing of Consumer Products with Low-cost 3D Printing from Free and Open Source Designs. *Eur. J. Soc. Impact Circular Econ.* 2022, 3(2):1–24.

[23] Publishing SM. New SmarTech Analysis Report on Additive Manufacturing in the Oil and Gas Industry Finds $1B+ Opportunity for AM Hardware Manufacturers. 2019. Available: https://www.globenewswire.com/news-release/2019/06/04/1864243/0/en/New-SmarTech-Analysis-Report-on-Additive-Manufacturing-in-the-Oil-and-Gas-Industry-Finds-1B-Opportunity-for-AM-Hardware-Manufacturers.html (accessed on 24 October 2023).

[24] Editor. Is PLA Recyclable? 2020. Available: https://bioplasticsnews.com/2020/04/05/is-pla-recyclable/ (accessed on 2 June 2024).

[25] Santander P, Cruz Sanchez FA, Boudaoud H, Camargo M. Closed loop supply chain network for local and distributed plastic recycling for 3D printing: a MILP-based optimization approach. *Resour. Conserv. Recycl.* 2020, 154:104531.

[26] Dertinger SC, Gallup N, Tanikella NG, Grasso M, Vahid S, *et al.* Technical pathways for distributed recycling of polymer composites for distributed manufacturing: Windshield wiper blades. *Resour. Conserv. Recycl.* 2020, 157:104810.
[27] Woern AL, McCaslin JR, Pringle AM, Pearce JM. RepRapable Recyclebot: Open source 3-D printable extruder for converting plastic to 3-D printing filament. *HardwareX* 2018, 4:e00026.
[28] Anderson I. Mechanical Properties of Specimens 3D Printed with Virgin and Recycled Polylactic Acid. *3D Print. Addit. Manuf.* 2017, 4(2):110–115.
[29] Vidakis N, Petousis M, Tzounis L, Grammatikos SA, Porfyrakis E, *et al.* Sustainable Additive Manufacturing: Mechanical Response of Polyethylene Terephthalate Glycol over Multiple Recycling Processes. *Materials* 2021, 14(5):1162.
[30] Cruz Sanchez FA, Boudaoud H, Hoppe S, Camargo M. Polymer recycling in an open-source additive manufacturing context: Mechanical issues. *Addit. Manuf.* 2017, 17:87–105.
[31] Petsiuk A, Pearce JM. Open Source Filament Diameter Sensor for Recycling, Winding, and Additive Manufacturing Machines. *J. Manuf. Sci. Eng.* 2021, 143(10):105001.
[32] Song H, Martínez J, Bedell P, Vennin N, Lefebvre S. Colored Fused Filament Fabrication. *ACM Trans. Graph.* 2019, 38(5):1–11.
[33] Wittbrodt B, Pearce JM. The effects of PLA color on material properties of 3-D printed components. *Addit. Manuf.* 2015, 8:110–116.
[34] Caceres-Mendoza C, Santander-Tapia P, Cruz Sanchez FA, Troussier N, Camargo M, *et al.* Life cycle assessment of filament production in distributed plastic recycling via additive manufacturing. *Cleaner Waste Syst.* 2023, 5:100100.
[35] FAST. SpecOptiBlend. 2023. Available: https://osf.io/92wu6/ (accessed on 12 March 2025).
[36] Bullett TR. 17 - Appearance qualities of paint — Basic concepts. In *Paint and Surface Coatings*, 2nd ed. Cambridge: Woodhead Publishing, 1999. pp. 621–641.
[37] Anon. Python.org. 2023. Available: https://www.python.org/ (accessed on 2 June 2024).
[38] Anon. SciPy. 2024. Available: https://scipy.org/ (accessed on 30 October 2023).
[39] Nelder JA, Mead R. A Simplex Method for Function Minimization. *Comput. J.* 1965, 7(4):308–313.
[40] Wright M. Direct search methods: Once scorned, now respectable. In *Numerical analysis*, Harlow: Addison-Wesley, 1996. pp. 191–208.
[41] Nicholson H. Sequential Least-Squares Estimation, Identification, Reduction and Control. Part 2. 1969. Available: https://eprints.whiterose.ac.uk/75885/ (accessed on 6 November 2023).
[42] Hodson TO. Root-mean-square error (RMSE) or mean absolute error (MAE): when to use them or not. *Geosci. Model Dev.* 2022, 15(14):5481–5487.
[43] Sharma G, Wu W, Dalal EN. The CIEDE2000 color-difference formula: Implementation notes, supplementary test data, and mathematical observations. *Color Res. Appl.* 2004, 30(1):21–30.
[44] Anon. CIE, International Commission on Illumination, Comission internationale de l'Eclairage, Internationale Beleuchtungskommission. 2023. Available: https://cie.co.at/ (accessed on 12 March 2025).
[45] Wee AG, Lindsey DT, Shroyer KM, Johnston WM. Use of a porcelain color discrimination test to evaluate color difference formulas. *J. Prosthet. Dent.* 2007, 98(2):101–109.
[46] Berns RS. *Billmeyer and Saltzman's Principles of Color Technology*. Hoboken: John Wiley & Sons, 2019.

[47] Berns RS, Mohammadi M. Single-constant simplification of Kubelka-Munk turbid-media theory for paint systems—A review. *Color Res. Appl.* 2007, 32(3):201–207.
[48] Walowit E, McCarthy CJ, Berns RS. An algorithm for the optimization of kubelka-munk absorption and scattering coefficients. *Color Res. Appl.* 1987, 12(6):340–343.
[49] Berns R, Mohammadi M. Evaluating Single- and Two-Constant Kubelka-Munk Turbid Media Theory for Instrumental-Based Inpainting. *Stud. Conserv.* 2007, 52:299–314.
[50] Walowit E, McCarthy CJ, Berns RS. An algorithm for the optimization of kubelka-munk absorption and scattering coefficients. *Color Res. Appl.* 1987, 12(6):340–343.
[51] Anon. Polymaker CA – 3D Printing Filament for your 3D Printer. Available: https://ca.polymaker.com/ (accessed on 12 March 2025).
[52] Anon. Filabot Reclaimer. 2024. Available: https://www.filabot.com/products/filabot-reclaimer-1 (accessed on 29 October 2023).
[53] Woods MC, Kulkarni A, Pearce JM. The Potential of Replacing Concrete with Sand and Recycled Polycarbonate Composites: Compressive Strength Testing. *J. Compos. Sci.* 2023, 7(6):249.
[54] Woods MC, Brooks CK, Pearce JM. Open-source cold and hot scientific sheet press for investigating polymer-based material properties. *HardwareX* 2024, 19.
[55] Labmate I. Reflectance Spectroscopy - A Useful Technique for Analysing Solid Samples. 2022, Available: http://www.labmate-online.com/article/mass-spectrometry-and-spectroscopy/41/ocean-insight-inc/reflectance-spectroscopy-a-useful-technique-for-analysing-solid-samples/3099 (accessed on 7 November 2023).
[56] Anon. Optical Fibers, Ocean Insight. 2023. Available: https://www.oceaninsight.com/products/fibers-and-probes/fibers/ (accessed on 9 October 2023).
[57] Anon. ReDeTec. 2023, Available: https://redetec.com/pages/downloads-and-documentation (accessed on 29 April 2024).
[58] Anon. Color-Hex. 2023. Available: https://www.color-hex.com/color/49257d (accessed on 12 March 2025).
[59] Anon. CMYK value of the Western Purple. 2024. Available: https://www.colorhexa.com/4f2683 (accessed on 12 March 2025).
[60] Myers DE. Spatial interpolation: an overview. *Geoderma* 1994, 62(1):17–28.
[61] Ibraheem NA, Hadan MM, Khan RZ, Mishra PK. Understanding color models: a review. *ARPN J. of Sci. Technol.* 2012, 2(3):265–275.
[62] Rosentrater KA, Evers AD. Flour treatments, applications, quality, storage and transport. In *Kent's Technology of Cereals*, 5th ed. Cambridge: Woodhead Publishing, 2018. pp. 515–564.
[63] Phillips K. What Is CIELAB Color Space? 2023. Available: https://www.hunterlab.com/blog/what-is-cielab-color-space/ (accessed on 29 October 2023).
[64] Whelan B, Loo Jr BW, Wang J, Keall P. TopasOpt: an open-source library for optimization with Topas Monte Carlo. *Med. Phys.* 2023, 50(2):1121–1131.
[65] Zhu C, Byrd RH, Lu P, Nocedal J. Algorithm 778: L-BFGS-B: Fortran subroutines for large-scale bound-constrained optimization. *ACM Trans. Math. Softw.* 1997, 23(4):550–560.
[66] Byrd RH, Lu P, Nocedal J, Zhu C. A Limited Memory Algorithm for Bound Constrained Optimization. *SIAM J. Sci. Comput.* 1995, 16(5):1190–1208.

[67] Ma Y, Zhang N, Li J. Improved Sequential Least Squares Programming–Driven Feasible Path Algorithm for Process Optimisation. In *Computer Aided Chemical Engineering*, Amsterdam: Elsevier, 2022. pp. 1279–1284.
[68] Brown StevenD, Tauler R, Walczak B. *Comprehensive Chemometrics*, 1st ed. Amsterdam: Elsevier, 2009.
[69] Anon. Wildflower Bouquet. 2024. Available: https://www.lego.com/en-ca/product/wildflower-bouquet-10313 (accessed on 12 March 2025).
[70] Patel DK, Zhong K, Xu H, Islam MF, Yao L. Sustainable Morphing Matter: Design and Engineering Practices. *Adv. Mater. Technol.* 2023, 8(23):2300678.
[71] Machado CG, Winroth MP, Ribeiro da Silva EHD. Sustainable manufacturing in Industry 4.0: an emerging research agenda. *Int. J. Prod. Res.* 2020, 58(5):1462–1484.
[72] Suescun C, Cruz F, Boudaoud H, Joahua M. P, Hoppe S, *et al.* Compatibilizer Effectiveness for the Reuse of Mixed Post-Consumersolid Waste Towards Distributed Recycling. *Addit. Manuf.* (in press)
[73] Laganovska K, Zolotarjovs A, Vázquez M, Mc Donnell K, Liepins J, *et al.* Portable low-cost open-source wireless spectrophotometer for fast and reliable measurements. *HardwareX* 2020, 7:e00108.
[74] Anon. OpenRAMAN. 2024. Available: https://www.open-raman.org/ (accessed on 12 March 2025).
[75] Gaudi. Open Fiber Spectrometer. 2024. Available: http://www.gaudi.ch/GaudiLabs/?page_id=825 (accessed on 24 June 2024).
[76] Public Lab. Spectrometry. 2024. Available: https://publiclab.org/n/16 (accessed on 24 June 2024).
[77] Anon. ColorZilla - Eyedropper, Color Picker, Gradient Generator and more. Available: https://www.colorzilla.com/ (accessed on 2 November 2023).
[78] Mohammed M, Wilson D, Gomez-Kervin E, Petsiuk A, Dick R, *et al.* Sustainability and feasibility assessment of distributed E-waste recycling using additive manufacturing in a Bi-continental context. *Addit. Manuf.* 2022, 50:102548.
[79] Zhong S, Rakhe P, Pearce JM. Energy Payback Time of a Solar Photovoltaic Powered Waste Plastic Recyclebot System. *Recycling* 2017, 2(2):10.
[80] Mohammed MI, Wilson D, Gomez-Kervin E, Vidler C, Rosson L, *et al.* The Recycling of E-Waste ABS Plastics by Melt Extrusion and 3D Printing Using Solar Powered Devices as a Transformative Tool for Humanitarian Aid. In *Proceedings of the 29th Annual International Solid Freeform Fabrication Symposium – An Additive Manufacturing Conference*, Austin, USA, August 13–15, 2018, pp. 80–92.
[81] King DL, Babasola A, Rozario J, Pearce JM. Mobile Open-Source Solar-Powered 3-D Printers for Distributed Manufacturing in Off-Grid Communities. *Challenges Sustainability* 2014, 2(1):18–27.
[82] Wong JY. Ultra-Portable Solar-Powered 3D Printers for Onsite Manufacturing of Medical Resources. *Aerosp. Med. Hum. Perform.* 2015, 86(9):830–834.
[83] Gwamuri J, Franco D, Khan KY, Gauchia L, Pearce JM. High-Efficiency Solar-Powered 3-D Printers for Sustainable Development. *Machines* 2016, 4(1):3.
[84] Mohammed MI, Wilson D, Gomez-Kervin E, Rosson L, Long J. EcoPrinting: Investigation of Solar Powered Plastic Recycling and Additive Manufacturing for Enhanced Waste Management

and Sustainable Manufacturing. In *2018 IEEE Conference on Technologies for Sustainability (SusTech)*, Long Beach, USA, November 11–13, 2018, pp. 1–6.

[85] Cress AK, Huynh J, Anderson EH, O'neill R, Schneider Y, *et al.* Effect of recycling on the mechanical behavior and structure of additively manufactured acrylonitrile butadiene styrene (ABS). *J. Cleaner Prod.* 2021, 279:123689.

[86] Mohammed MI, Wilson D, Gomez-Kervin E, Tang B, Wang J. Investigation of Closed-Loop Manufacturing with Acrylonitrile Butadiene Styrene over Multiple Generations Using Additive Manufacturing. *ACS Sustainable Chem. Eng.* 2019, 7(16):13955–13969.

[87] Chong S, Pan GT, Khalid M, Yang TCK, Hung ST, *et al.* Physical Characterization and Pre-assessment of Recycled High-Density Polyethylene as 3D Printing Material. *J. Polym Environ* 2017, 25(2):136–145.

[88] Pepi M, Zander N, Gillan M. Towards Expeditionary Battlefield Manufacturing Using Recycled, Reclaimed, and Scrap Materials. *JOM* 2018, 70.

[89] Oblak P, Gonzalez-Gutierrez J, Zupančič B, Aulova A, Emri I. Processability and mechanical properties of extensively recycled high density polyethylene. *Polym. Degrad. Stab.* 2015, 114:133–145.

[90] Oberloier S, Whisman NG, Pearce JM. Finding Ideal Parameters for Recycled Material Fused Particle Fabrication-Based 3D Printing Using an Open Source Software Implementation of Particle Swarm Optimization. *3D Print. Addit. Manuf.* 2023, 10(6):1287–1300.

[91] Woern AL, Pearce JM. Distributed Manufacturing of Flexible Products: Technical Feasibility and Economic Viability. *Technologies* 2017, 5(4):71.

[92] Lee JH, Lim KS, Hahm WG, Kim SH. Properties of recycled and virgin poly (ethylene terephthalate) blend fibers. *J. Appl. Polym. Sci.* 2013, 128(2):1250–1256.

[93] Little HA, Tanikella NG, J. Reich M, Fiedler MJ, Snabes SL, *et al.* Towards Distributed Recycling with Additive Manufacturing of PET Flake Feedstocks. *Materials* 2020, 13(19):4273.

[94] Reich MJ, Woern AL, Tanikella NG, Pearce JM. Mechanical Properties and Applications of Recycled Polycarbonate Particle Material Extrusion-Based Additive Manufacturing. *Materials* 2019, 12(10):1642.

[95] Zander NE. Recycled Polymer Feedstocks for Material Extrusion Additive Manufacturing. In *Polymer-Based Additive Manufacturing: Recent Developments*, Washington, D.C.: American Chemical Society, 2019. pp. 37–51.

[96] Parandoush P, Lin D. A review on additive manufacturing of polymer-fiber composites. *Compos. Struct.* 2017, 182:36–53.

[97] Heller BP, Smith DE, Jack DA. Planar deposition flow modeling of fiber filled composites in large area additive manufacturing. *Addit. Manuf.* 2019, 25:227–238.

[98] Rahimizadeh A, Kalman J, Henri R, Fayazbakhsh K, Lessard L. Recycled Glass Fiber Composites from Wind Turbine Waste for 3D Printing Feedstock: Effects of Fiber Content and Interface on Mechanical Performance. *Materials* 2019, 12(23):3929.

[99] Sam-Daliri O, Ghabezi P, Steinbach J, Flanagan T, Finnegan W, *et al.* Experimental study on mechanical properties of material extrusion additive manufactured parts from recycled glass fibre-reinforced polypropylene composite. *Compos. Sci. Technol.* 2023, 241:110125.

[100] Tian X, Liu T, Wang Q, Dilmurat A, Li D, *et al*. Recycling and remanufacturing of 3D printed continuous carbon fiber reinforced PLA composites. *J. Cleaner Prod.* 2017, 142:1609–1618.

[101] Zander NE, Gillan M, Burckhard Z, Gardea F. Recycled polypropylene blends as novel 3D printing materials. *Addit. Manuf.* 2019, 25:122–130.

[102] Romani A, Levi M, Pearce JM. Recycled polycarbonate and polycarbonate/acrylonitrile butadiene styrene feedstocks for circular economy product applications with fused granular fabrication-based additive manufacturing. *Sustainable Mater.Technol.* 2023, 38:e00730.